Cell Reports, Volume *35*

Supplemental information

Hepatitis C virus drugs that inhibit SARS-CoV-2 papain-like protease synergize with remdesivir to suppress viral replication in cell culture

Khushboo Bafna, Kris White, Balasubramanian Harish, Romel Rosales, Theresa A. Ramelot, Thomas B. Acton, Elena Moreno, Thomas Kehrer, Lisa Miorin, Catherine A. Royer, Adolfo García-Sastre, Robert M. Krug, and Gaetano T. Montelione

Inhibitor	Identifier of Protease Inhibitor	Database ID of Protease Inhibitor Structure	*AutoDock* Score (kcal/mol) Lowest "Energy"	
			M^{pro}	PL^{pro}
SARS-CoV-2 M^{pro} Inhibitor				
α-ketoamide inhibitor 13b				
lowest "energy" pose	06K	6Y2G[a]	-9.17	Not Applicable
pose most similar to X-ray structure:			-9.03	
SARS-CoV-2 PL^{pro} Inhibitor				
GRL0167				
lowest "energy" pose		7CJM[a]	Not Applicable	-7.54
HCV NSP3/4A Protease Inhibitor Drugs				
vaniprevir	VAN	3SU3[c]	-10.95	-7.85
simeprevir	SIM	3KEE[c]	-10.75	-8.12
paritaprevi	PAR	32700634[b]	-10.71	-10.30
danoprevi	DAN	3M5L[c]	-9.99	-8.48
narlaprevir	NAR	3LON[c]	-9.80	-5.56
grazoprevi	GRZ	3SUD[c]	-9.71	-8.10
glecaprevir	GLE	35013015 [b]	-9.51	-8.30
boceprevir	BOC	10324367[d]	-9.13	-5.56
telaprevir	TEL	3SV6[c]	-9.05	-6.57
asunaprevir	ASU	4WF8[c]	-8.37	-6.57

Supplementary Table S1. AutoDock docking scores for SARS-CoV-2 M^{pro} and HCV NS3/4A protease inhibitors. Related to Figure panels 1A-D, Figure 6A, and STAR Methods. (a) Atomic coordinates for the inhibitor were taken from listed PDB id. (b) Atomic coordinates for the inhibitor were taken from the ChemSpider database. (c) Atomic coordinates for the inhibitor were taken from the PDB coordinates of the corresponding complex of the inhibitor bound to HCV NS3/4A protease. (d) Atomic coordinates for the inhibitor were taken from the Pubchem database.

			Vero E6 Cells		HEK 293T Cells			
	Relative M^{pro} Inhibition[a]	**Relative PL^{pro} Inhibition[a]**	**IC_{50}**	**CC_{50}**	**IC_{50}**	**CC_{50}**	**Synergy Score**	
BOC	strong	none	19.6	>50	5.4	>50	-7.6	additive
NAR	strong	none	7.7	>20	15.0	72.0	-3.6	additive
TEL	strong	none	>50	>50	20.5	>50	-	not tested
SIM	moderate	strong	4.2	2.1	2.3	>50	+30.2	synergistic
VAN	strong	strong	6.2	4.3	3.0	>50	+10.9	synergistic
PAR	none	moderate	6.0	>100	0.55	>100	+17.3	synergistic
GRZ	moderate	moderate	10.8	>50	16.7	>50	+25.0	synergistic
ASU	moderate	none	15.0	48.9	48.4	>50	-	not tested
GLE	none	none	>50	>50	>50	>50	-	not tested
DAN	none	none	>50	>50	>50	31.1	-	not tested

Supplementary Table S2. **Comparison of enzyme inhibition and viral inhibition activities of HCV protease inhibitors**. Related to Figures 1, 2, 3, 4, 5, and 6. (a) Strong inhibition corresponds to an estimated IC_{50} < about 20 μM, moderate inhibition corresponds to an estimated IC_{50} in the range 20 – 50 μM, and none indicates no observed inhibition of protease activity at drug concentrations of 50 μM.

.

Drug or Inhibitor Molecule	M^{pro} Assay		PL^{pro} Assay	
	OD_{360} of reaction mixture	Inner filter correction factor	OD_{360} of reaction mixture	Inner filter correction factor
BOC	0.0143	1.000	0.0053	1.000
NAR	0.0114	1.000	0.0024	1.000
TEL	0.0112	1.000	0.0022	1.000
SIM	0.0201	1.000	0.0111	1.000
VAN	0.0398	1.300	0.0308	1.125
PAR	0.0159	1.000	0.0068	1.000
GRZ	0.0161	1.000	0.0071	1.000
ASU	0.0197	1.000	0.0107	1.000
GLE	0.0191	1.000	0.0101	1.000
DAN	0.0126	1.000	0.0036	1.000

Supplementary Table S3. Inner filter effect corrections to fluorescence-based enzyme assays. Related to Figures 1B, 1E, 5B, 6A, and 6B, and STAR Methods. The inner filter effect was assessed by measuring fluorescence and emission for the fluorescent dye diethylamino naphthalene sulfonate (DENS) over the range 0.01 to 1.0 O.D. units, at the excitation wavelength (360 nm), using the Infinite M1000 TECAN plate reader. In this microtiter plate system, inner filter effects are negligible for A_{360} values below ~ 0.025 OD units. For each of the fluorescent peptide substrate (20 μM) / drug (20 μM) mixtures, the A_{360} was measured, and compared with fluorescence emission vs absorbance data obtained on a control fluorophore dye, DENS, to determine the inner filter effect correction value. At these peptide and drug concentrations, only the vaniprevir drug peptide mixtures required inner-filter effect corrections.

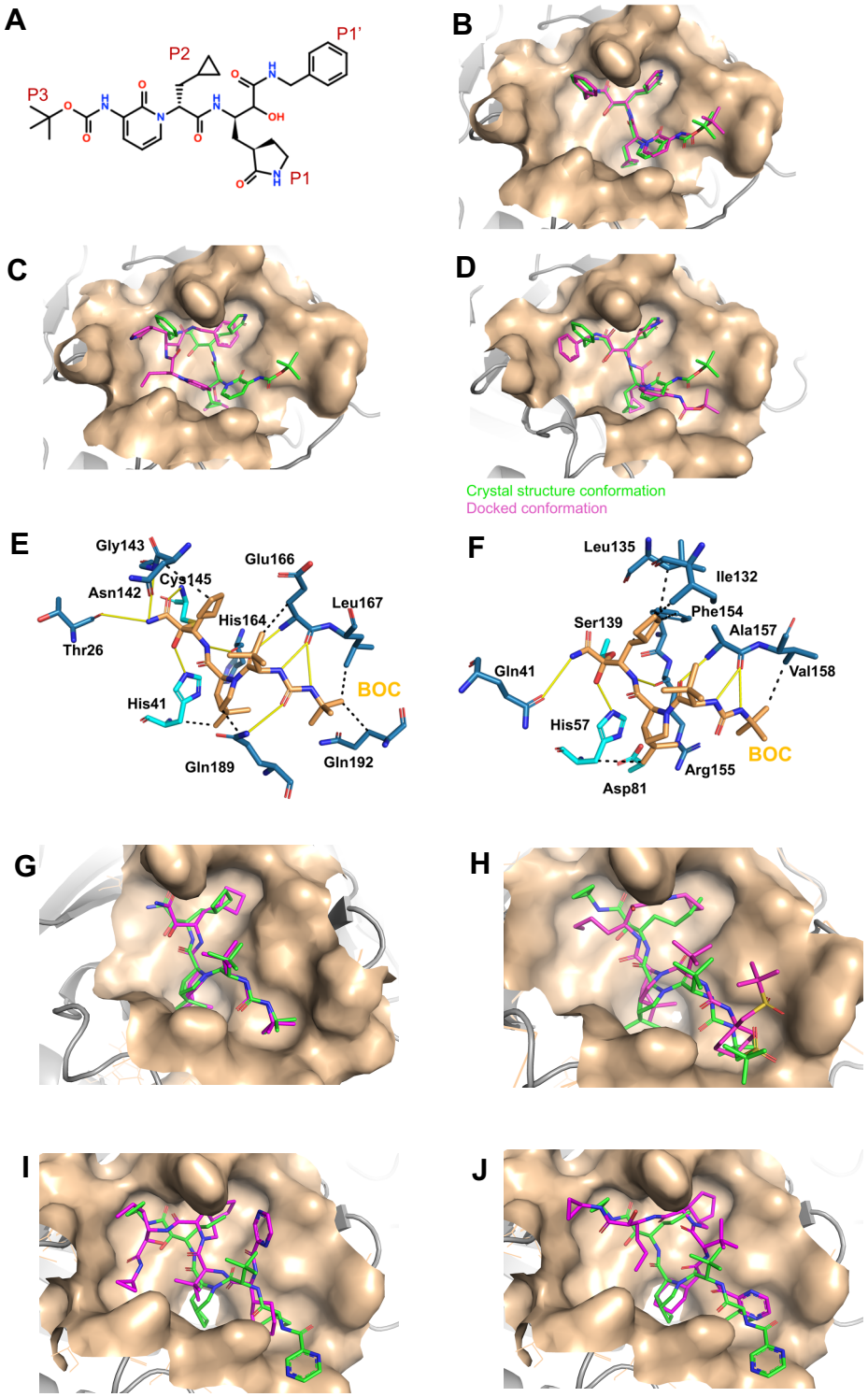

Fig. S1. Comparison of covalent inhibitor complexes of *AutoDock* with subsequently determined X-ray crystal structures. Related to Figures 1A-G, Figures 5A-B, and STAR Methods. (A) Chemical structure of α-ketoamide inhibitor 13b, in the alcohol form resulting from forming hemithioketal with Cys thiol of M^{pro} (Zhang et al., 2020b). (B) Lowest "energy" *AutoDock* pose using a rigid conformation of α-ketoamide inhibitor 13b, in order to match the ligand conformation in X-ray crystal structure of the complex (score = -7.19 kcal/mol). (C) Lowest "energy" *AutoDock* pose observed among 100 docking simulations (score = -9.17 kcal/mol). (D) The low "energy" *AutoDock* pose (score = -9.03 kcal/mol) of 13b that is most similar to the conformation seen in the crystal structure. In panels B-D, M^{pro} is shown in surface representation, X-ray crystal structure of α-ketoamide inhibitor 13b bound in the active site of M^{pro} in green sticks (PDB id 6Y2G), and the predicted *AutoDock* conformation in magenta sticks. (E) Details from the X-ray crystal

structure of the SARS-CoV-2 M^{pro} protease - boceprevir (BOC) complex [PDB id 6WNP, (Anson et al., 2020)]. (F) Details from the X-ray crystal structure of the HCV NS3/4A protease - BOC complex [(PDB id 2OC8, (Prongay et al., 2007)]. In both of these boceprevir – protease complex structures, remarkable similarity is observed between the binding poses and protein-inhibitor hydrogen bond networks. In the complex with HCV protease, boceprevir forms hydrogen bonds with side chains of residues Gln41 and His57 and with backbone atoms of Gly137, Ser139, Arg155 and Ala157. The corresponding residue equivalents (based on structural superimposition) of these residues in M^{pro}, Thr26, His41, Gly143, Cys145, His164 and Glu166, also form hydrogen bonds with boceprevir. The sidechain of residue Gln189 of SARS-CoV-2 M^{pro} forms an additional hydrogen-bond with boceprevir. (G) BOC binding pose in best-scoring *AutoDock* complex (magenta) compared with the X-ray crystal structure of a second BOC-M^{pro} complex [green, PDB id 6XQU, (Kneller et al., 2020a). (H) Narleprevir (NAR) binding pose in best-scoring *AutoDock* complex (magenta) compared with the X-ray crystal structure of the NAR-M^{pro} complex [green, PDB id 6XQT, (Kneller et al., 2020a). (I) Telaprevir (TEL) binding pose in second-best-scoring *AutoDock* complex (magenta) compared with the X-ray crystal structure of TEL-M^{pro} complex (green, PDB id 6XQS, (Kneller et al., 2020a). (J) TEL binding pose in 37^{th}-ranked *AutoDock* complex (magenta) compared with the X-ray crystal structure of TEL-M^{pro} complex [green, PDB id 6XQS, (Kneller et al., 2020a).

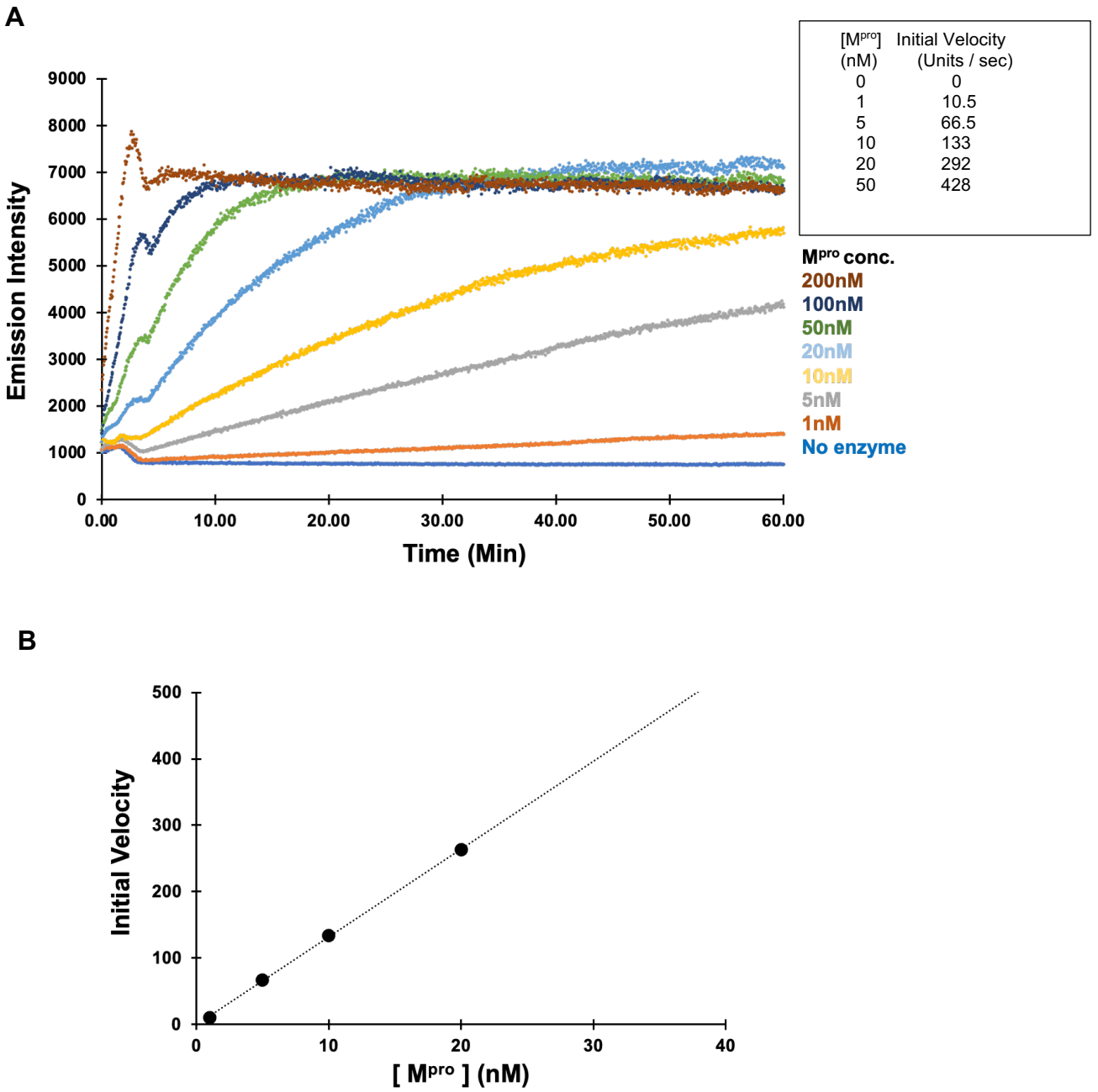

Fig. S2. Features of M^{pro} FRET proteolysis assay. Related to Figure 1E, and STAR Methods. (A) M^{pro} protease activity vs enzyme concentration using substate Dabsyl-KTSAVLQ/SGFRKME-Edans at pH 6.5 and 25 ºC, over the range of 0 to 200 nM M^{pro} concentration. Initial rates of hydrolysis measured at 0 to 50 nM enzyme concentration are indicted in the inset; at higher concentrations the rates were too fast to measure. For time points < 3 min, equilibration artifacts prevent reliable measurements. (B) Rates of hydrolysis (units / sec) are linear over the range 0 to 20 nM M^{pro} concentration.

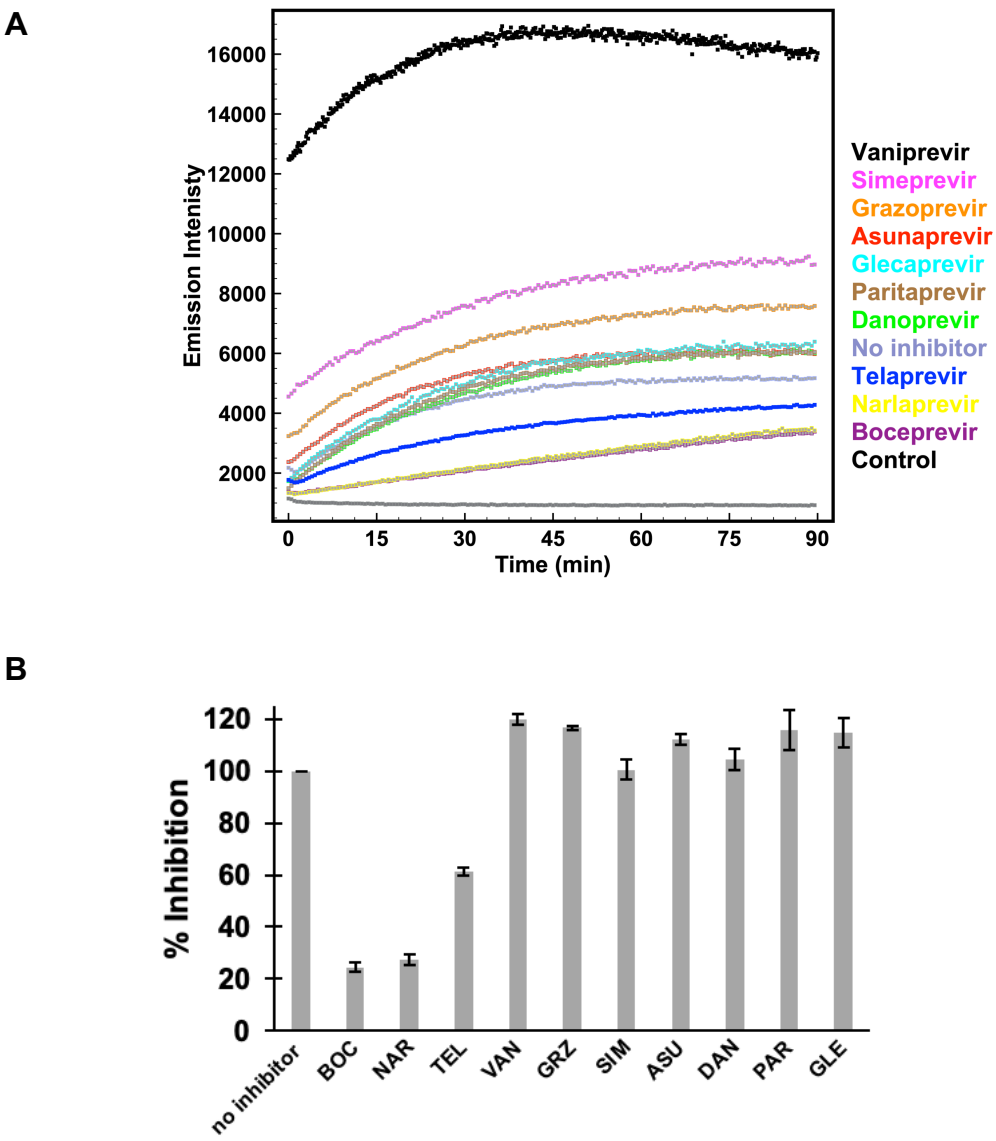

Fig. S3. SARS-CoV2 M^{pro} inhibition by HCV protease inhibitors. Related to Figure 1E, and STAR Methods. (A) Progression kinetics for M^{pro} were monitored in a FRET assay using substate Dabsyl-KTSAVLQ/SGFRKME-Edans at pH 6.5 and 25 ºC, under conditions outlined in the Star Methods. (B) Initial rates of proteolysis of a peptide substrate by M^{pro} in the presence of 20 μM inhibitor concentrations (v_i) relative to initial rate in the absence of inhibitor ($v_{i,o}$). Data for vaniprevir (VAN) has been corrected for inner filter effects, as outlined in STAR Methods and Supplementary Table S3.

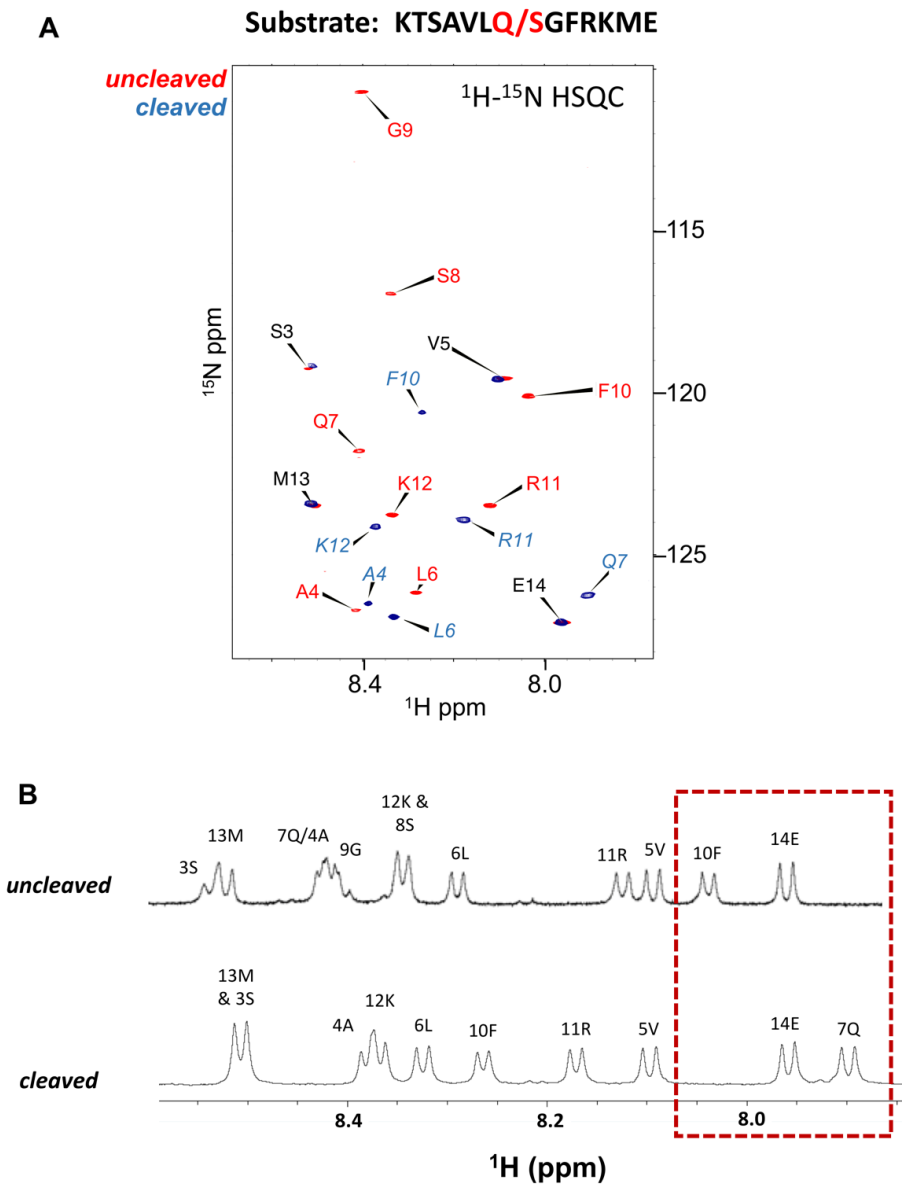

Fig. S4. Chemical shift assignments of backbone amide protons in uncleaved and cleaved M^{pro} peptide substrate. Related to Figures 1F-G, and STAR Methods. (A) Overlay of 2D ^{1}H-^{15}N HSQC spectra for uncleaved (red) and cleaved (blue) peptides (B) 1D ^{1}H spectra for cleaved and uncleaved peptides. Both spectra show changes in chemical shifts for some amino acids indicating proteolytic cleavage. These chemical shifts were determined at 25 °C using 2D COSY, TOCSY, and ^{1}H-^{15}N HSQC, along with 1D ^{1}H NMR experiments.

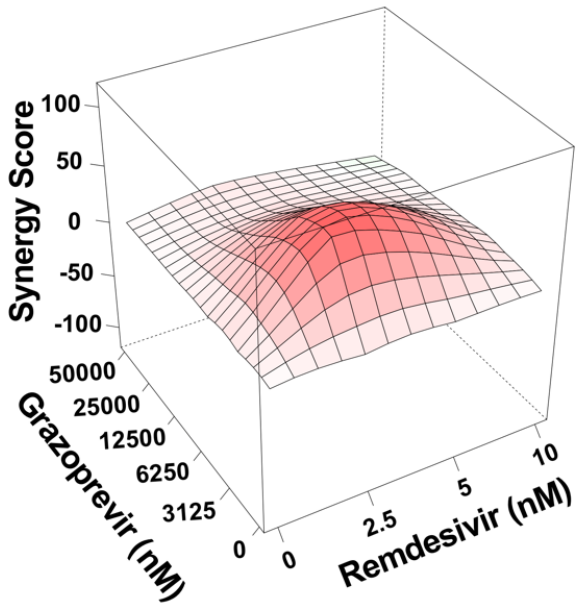

Fig. S5. Grazoprevir is also synergistic with remdesivir in an antiviral combination assay in human 293T cells. Related to Fig. 4. Human 293T cells were infected with SARS-CoV-2 in presences of two compounds titrated against each other in 2-fold serial dilutions and viral replication was determined using the immunofluorescence-based assay. As in Vero E6 cells (synergy score + 25.0), grazoprevir has positive ZIP synergy score (Ianevski et al., 2020) of + 20.3, indicative of its synergy with remdesivir.

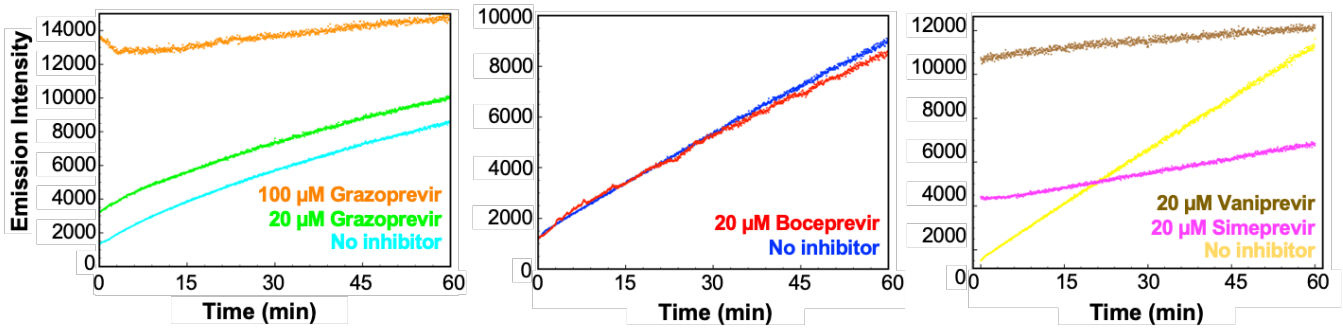

Fig S6. SARS-CoV-2 PL^{pro} inhibition by HCV protease inhibitors. Related to Figure 5B, and STAR Methods. Progression kinetics for PL^{pro} were monitored in a florescence assay using the fluorogenic substrate zRLRGG/AMC, at pH 7.5 and 25 ^{o}C, as outline in STAR Methods. 20 nM of PL^{pro} was incubated with 20 µM of HCV drugs. 20 µM substrate was added and the reaction was monitored for 2 hrs using the Infinite M1000 TECAN plate reader with filters for excitation at 360 nm and emission at 460 nm. These data document PL^{pro} inhibition by simeprevir and vaniprevir at 20 µM drug concentration, and grazoprevir at 100 µM drug concentration, with initial slopes less than that obtained in the absence of inhibitor. Boceprevir at 20 µM concentration does not inhibit PL^{pro}. The offsets at t=0 of emission intensity are due to the intrinsic fluorescence of the drugs.

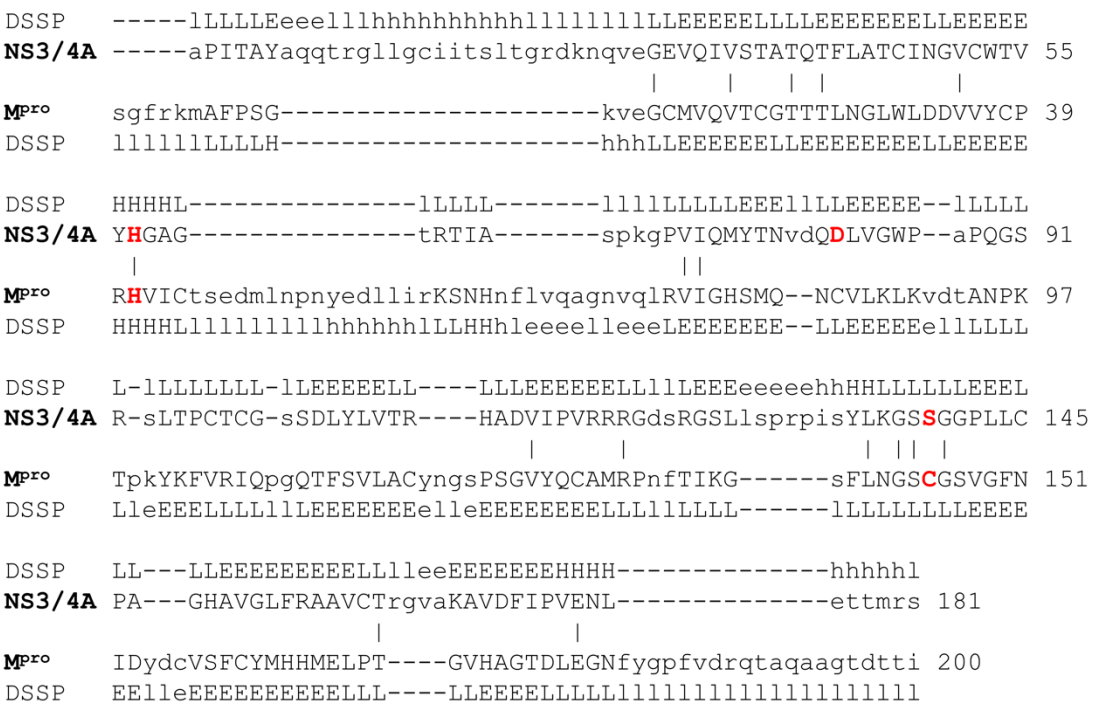

Fig. S7. Structure-based sequence alignment of HCV NS3/4A (NS3/4A) and SARS-CoV-2 M^{pro} (M^{pro}). Related to Figure 1A. The structure-based alignment results in alignment of key catalytic residues His41 and Cys145 of the SARS-CoV-2 M^{pro} with His57 and Ser139 of HCV NS3/4A protease, and some other substrate binding cleft residues. Catalytic residues of HCV NS3/4A (His57, Asp81 and Ser139) and SARS-CoV-2 M^{pro} (His41 and Cys145) are highlighted in bold red. Three-state secondary structure definitions by DSSP (H=helix, E=sheet, L=coil) are shown for each amino acid sequence. Structurally equivalent residues are in uppercase, structurally non-equivalent residues (e.g. in loops) are in lowercase. Identical amino acid are marked by vertical bars. This structure-based sequence alignment was generated using DALI (Holm and Sander, 1993, 1999).